Design Optimization of Linear-Rotary Motion Permanent Magnet Generator with E-type Stator

Kaikai Guo, *Member, IEEE,* and Youguang Guo, *Senior Member, IEEE*

***Abstract*—In order to meet the requirement of ocean energy power generation, a linear-rotary motion permanent magnet generator is proposed with E-type stator in the axial direction. The adjacent interlaced PM poles in the circumferential direction are staggered by half pole pitch in the axial direction, which are mounted on the surface of the mover. The rotary and linear motions are achieved by one magnetic circuit structure based on transverse flux principle and electromagnetic induction principle, respectively. The optimization design and electromagnetic characteristics of the proposed motor are analyzed by 3-D finite element method, and then the best optimization variable values are achieved. Compared with the results of the initial topology, the amplitude values of the cogging torque and detent force are reduced. Since three phases of the nine phase windings generate same initial phase angle of back electromagnetic force (back EMF) whether it works in rotary or linear motion, the traditional three phase energy storage system can be used to realize the energy storage of the nine phase windings, which reduces the difficulty of electrical energy storage. The variation of the amplitude of back EMF is hardly affected with different mover positions, which is conducive to improve the effective utilization of wave energy and tidal energy.**

***Index Terms*—Linear rotary permanent magnet machine; finite element method; interlaced pole; E-type stator structure**

I. Introduction

OCEAN energy power generation is one of the hottest spots of modern new energy power generation technology research. Linear rotary motion permanent magnet (PM) generator (LRMPMG) is an electromagnetic device that can generate electricity through linear and rotary motions, and it can effectively improve the efficiency of power generation, which have attracted much attentions. The motions of two-degree-of-freedom (2-DOF) direct drive induction motor were investigated, and the skewed slot method was applied to weaken the coupling effect in [1]. The torque and force characteristics of rotary-linear switched reluctance motor (RL-SRM) were analyzed by analytical and finite element methods (FEM) [2]. The key parameter, magnetic flux density and control system of flux reversal linear rotary PM machine were analyzed by magnetic circuit analytical model, analytical method and dual *dq* transformation method in [3-5]. A 2-DOF RL-SRM with decoupled magnetic structure was designed, and its control scheme was proposed to achieve a decoupled high positioning tracking accuracy [6]. To meet the high requirements of precision machining, a rotary-linear voice coil motor was proposed in [7]. An enhanced complex space vector based model of the rotary-linear machine with magnetic bearings was derived and the expressions for the torque, thrust and magnetic bearing force were reported in [8]. A linear rotary actuator with air-core coil mover was presented in [9], which can achieve high speed and dynamic response, and single-phase Lorentz-force driving scheme to realize direct and non-commutation actuation.

In order to improve the effective utilization rate of wave energy and tidal energy, a LRMPMG is proposed with E-type stator (ES) in the axial direction. The interlaced PM poles mounted on the surface of the mover are staggered by half pole pitch in the axial direction. The cogging torque, detent force, and back electromotive force (back EMF) are taken as the optimization objectives, and the optimization design is analyzed by 3-D FEM. Then the best optimization variable values are achieved. Compared with the results of the initial topology, the harmonic of back EMF, and the amplitudes of cogging torque and detent force are reduced.

II. Topology of ES-LRMPMG

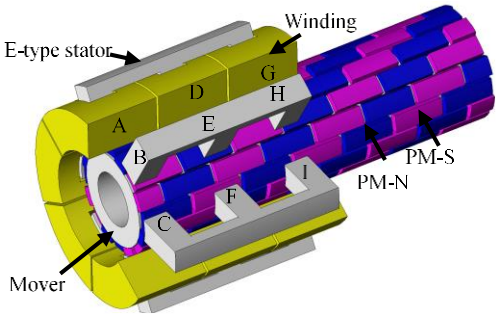

Fig. 1. Initial topology of ES-LRMPMG.

Fig. 1 shows the initial topology of ES-LRMPMG. The stator section consists of six E-type stators arrayed in the circumferential direction. The rotary and linear motions are achieved by only one magnetic circuit structure based on transverse flux and electromagnetic induction principles, respectively. The interlaced PM poles are staggered by half pole pitch in the axial direction. The phases (A, E, I), (B, F, G), and (C, D, H) have the same initial phase angle of back EMF waveform whether the motor works in rotary or linear motion, which can reduce the control strategy complexity.

Kaikai Guo is with the School of Electrical and Information Engineering & School of Mechanical Engineering, Anhui University of Science and Technology, Huainan, 232001, China (e-mail: guokai0072000@gmail.com).

Youguang Guo is with School of Electrical and Data Engineering, University of Technology Sydney, Sydney, NSW, 2007, Australia (e-mail: Youguang.guo-1@uts.edu.au).

Digital Object Identifier will be inserted here upon acceptance.

III. Optimization Design

A. Magnetic flux density analysis

Fig. 2 illustrates the magnetic flux density distribution of ES-LRMPMG at no load condition. It is seen that the end effect of the topology should be reduced by the optimization design of the motor. The magnetic flux density distributions in the circumferential stator tooth area and axial stator tooth area are shown in Fig. 3. The average values of the maximum value region in the circumferential and axial stator tooth areas are 0.9 T and 1.1 T, respectively.

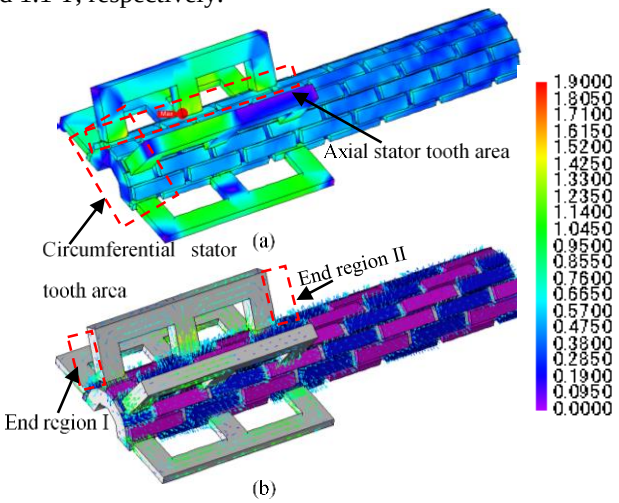

Fig. 2. Magnetic flux density distribution of ES-LRMPMG at no load condition, (a) contour plot, and (b) vector plot.

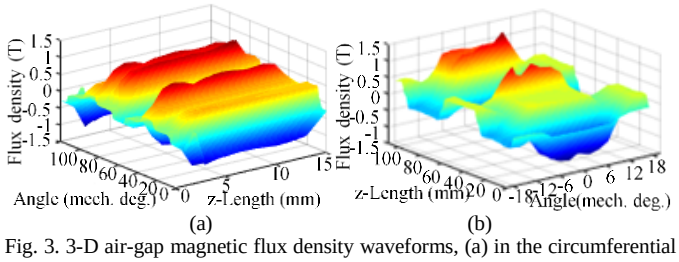

Fig. 3. 3-D air-gap magnetic flux density waveforms, (a) in the circumferential stator tooth area, and (b) in the axial stator tooth area.

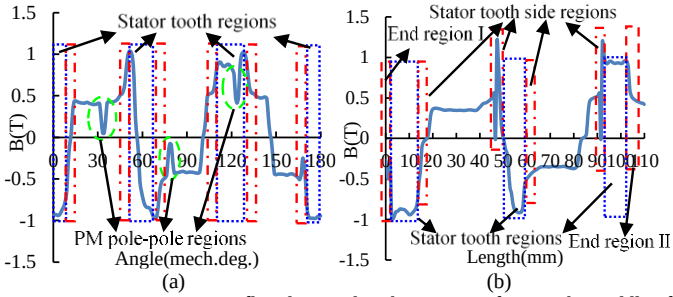

Fig. 4. 2-D air-gap magnetic flux density distribution waveform in the middle of (a) the circumferential stator pole region, and (b) the axial stator pole region.

In order to analyze the end effect and PM pole-pole regions, the air-gap magnetic flux density in the middle of the stator tooth area is shown in Fig. 4. The air-gap magnetic flux density can be suddenly changed when the magnetic field direction changes in the stator tooth side regions. In order to reduce the pole-pole flux leakage and harmonic of PM pole-pole regions, adjacent PM poles with the same magnetizing direction are taken as a whole, and the distance between the PM poles with different magnetizing directions is taken as the optimization object according to Figs. 2, 3 and 4. Then the topology is shown as Fig. 5 (a).

B. Optimization design

Figs. 5 (a) and (b) show the dimension structure diagrams of ES-LRMPMG. w_s and $w_{pm\theta}$ are the widths of stator pole and PM in the circumferential direction, respectively. w_{sa}, w_{spa}, w_{ga} and w_{pma} are the widths of stator pole, stator pole pitch, air gap width between the PM poles, and PM width in the axial direction, respectively. R_{so} and R_{si} are the radii of stator outside and inside, respectively. R_r, R_{sh} and R_{pm} are the radii of mover, mover shaft and PM, respectively. h_{sy} is the stator yoke height.

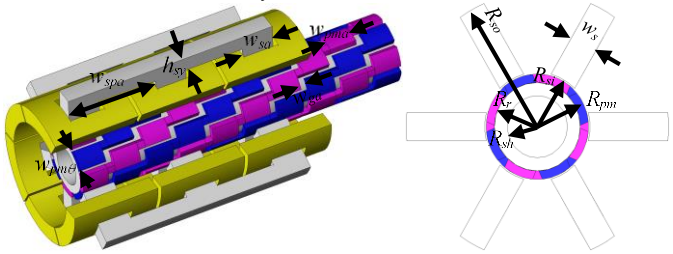

Fig. 5. Structure of ES-LRMPMG, (a) topology, (b) radial structure diagram.

According to the calculation methods of the PM height and the thickness of the stator yoke, the following calculation formulas can be derived

$$R_{pm} - R_r = u_r (R_{si} - R_{pm}) / (B_r / B_\delta - 1) \quad (1)$$

$$2B_{sy} p_\theta h_{sy} = B_\delta \pi R_{si} w_{pm} w_s / w_{sa} \quad (2)$$

where μ_r is the relative permeability of permanent magnets, B_r is the residual flux density of PM, B_δ is the average air-gap magnetic flux density, B_{sy} is the flux density in the stator yoke, p_θ is the number of pole pairs in the circumferential direction, and w_s and w_{sa} are the widths of the stator in the circumferential and axial directions, respectively.

According to the initial calculation, the selected optimization variables are divided into two sections. The first section consists of the parameters which can be achieved according to the power size equation of surface mounted permanent magnet synchronous motor, including R_{so}, R_{si}, R_r, R_{sh}, R_{pm} and h_{sy}. The second section consists of the parameters w_s, $w_{pm\theta}$, w_{sa}, w_{spa}, w_{ga} and w_{pma}. Since 3/4 pole-slot combination form is adopted, namely, $3*w_{spa}=4*(w_{ga}+w_{pma})$, the relationships of detent force and w_{sa}, w_{ga}, w_{spa}, cogging torque and w_s, $w_{pm\theta}$, w_{sa} are shown in Fig. 6, which are analyzed by 3-D FEM. Taking phase *E* as the analysis objective, Fig. 7 shows the fundamental content of back EMF of phase *E* related with w_s, $w_{pm\theta}$, $w_{ga,}$, w_{spa} and w_{sa} when it works in rotary or linear motion. Since the pole-pole flux leakage can generate large effect on the rotary back EMF of phase E when the mover is at the initial position, the fundamental content of rotary back EMF is less than that when it is in linear motion. The variation of $w_{pm\theta}$ can generate larger effect on back EMF than that generated by changing w_s when it works in rotary motion as shown in Fig. 7(a). According to Figs. 6 and 7, the values of w_{sa}, w_{ga}, w_{spa}, w_s, and $w_{pm\theta}$ are 18 mm, 6 mm, 46.5 mm, 10.5 mm, and 11 mm, respectively.

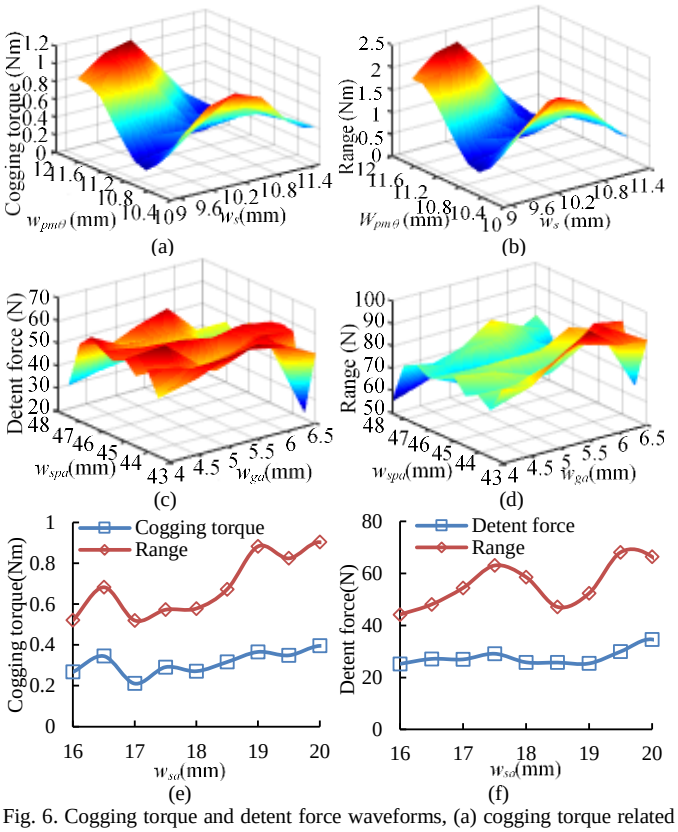

Fig. 6. Cogging torque and detent force waveforms, (a) cogging torque related with w_s, $w_{pm\theta}$, (b) cogging torque range related with w_s, $w_{pm\theta}$, (c) detent force related with w_{ga}, w_{spa}, (d) detent force range related with w_{ga}, w_{spa}, (e) cogging torque related with w_{sa}, and (f) detent force related with w_{sa}.

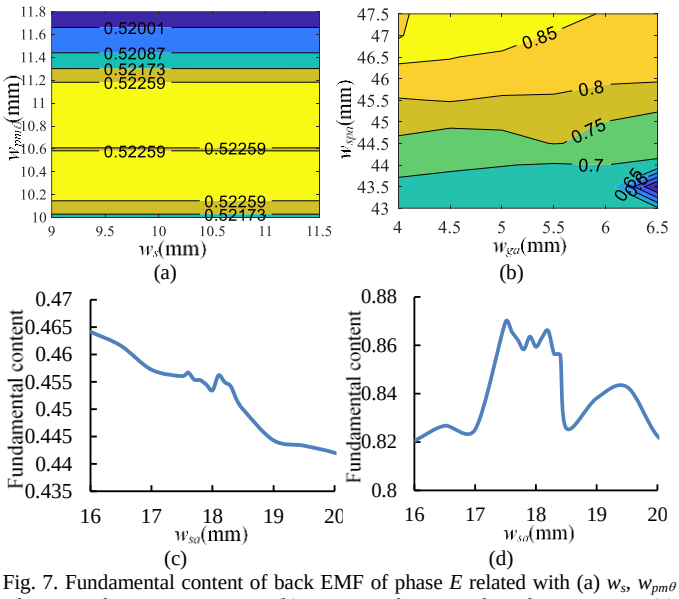

Fig. 7. Fundamental content of back EMF of phase *E* related with (a) w_s, $w_{pm\theta}$ when it works in rotary motion, (b) w_{ga}, w_{spa} when it works in linear motion, (c) w_{sa} when it works in rotary motion, and (d) w_{sa} when it works in linear motion.

According to the above analysis, the minimize value of the amplitude of cogging torque and detent force, the maximum value of fundamental content of the back EMF are taken as the optimization objective, and the best optimization variable values are achieved. Table I lists the main parameters of ES-LRMPMG.

TABLE I
MAIN PARAMETERS OF ES-LRMPMG

Parameters	*Value*	*Parameters*	*Value*	*Parameters*	*Value*
R_{so}(mm)	51	w_s(mm)	10.5	$w_{pm\theta}$(mm)	11
R_{si}(mm)	22.8	w_{sa}(mm)	18	w_{spa}(mm)	46.5
R_r(mm)	19.2	R_{pm}(mm)	22.2	w_{qa}(mm)	6
R_{sh}(mm)	11	h_{sy}(mm)	11	w_{pma}(mm)	34.9

IV. ANALYSIS OF ELECTROMAGNETIC CHARACTERISTICS

Assume the rated speeds of the rotary and linear motions are 1200 rpm and 1.4 m/s, respectively. Figs. 8 (a) and (b) show the back EMF waveforms when the machine is in rotary or linear motion. Figs. 8 (c) and (d) show the harmonic analysis results of back EMF when it works in rotary or linear motion. The main fundamental waveform contents of back EMF of phases *A*, *B* and *C* when the machine is in rotary motion are 0.67, 0.5 and 0.49, respectively. The main fundamental waveform contents of back EMF of phases *A*, *D* and *G* when it is in linear motion are 0.44, 0.6 and 0.59, respectively. It is seen that the initial phase angles of (*A*, *E*, *I*), (*C*, *D*, H) and (*B*, *F*, *G*) are the same, which can be stored by traditional electrical energy method.

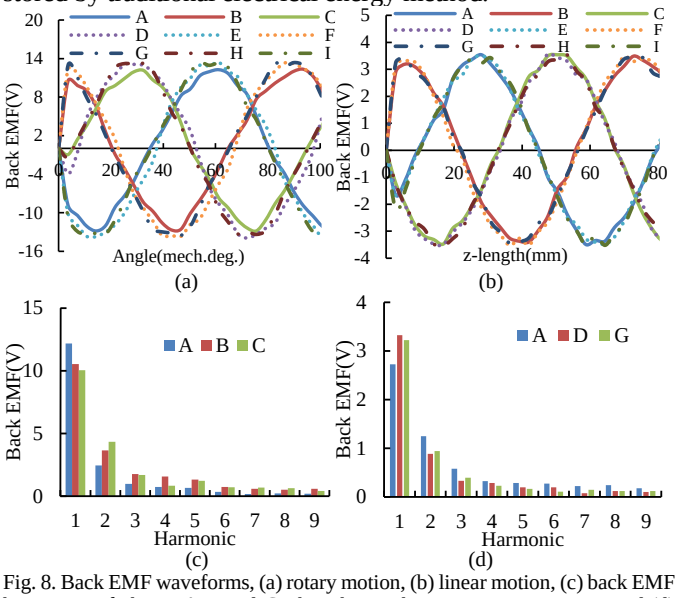

Fig. 8. Back EMF waveforms, (a) rotary motion, (b) linear motion, (c) back EMF harmonics of phases *A*, *B* and *C* when the machine is in rotary motion, and (d) back EMF harmonics of phases *A*, *D* and *G* when it is in linear motion.

Fig. 9 shows the cogging torque and detent force waveforms before and after the optimization. It is seen that the amplitudes of cogging torque and detent force are reduced compared to those of the initial topology by 32.86% and 37.48%, respectively. The amplitudes of cogging torque and detent force after the optimization are 0.557 Nm and 12.77 N, respectively.

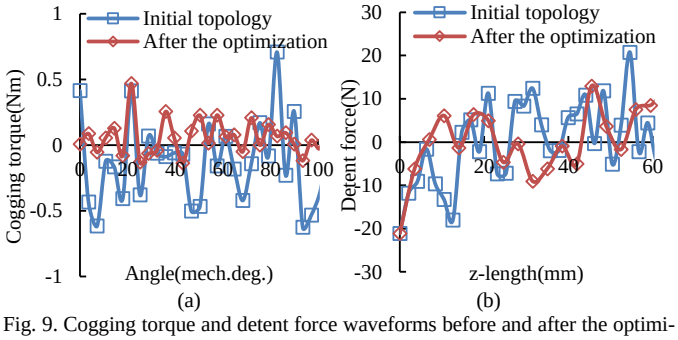

Fig. 9. Cogging torque and detent force waveforms before and after the optimization, (a) cogging torque, and (b) detent force.

Fig. 10 shows the air-gap flux density waveforms and harmonic analysis in the circumferential and axial directions. The main fundamental harmonics are 0.71 T and 0.65 T in the circumferential and axial directions, respectively. Fig. 11 shows the cogging torque and detent force when the motor works in rotary or linear motion at different positions. When the mover is at different positions, the cogging torque and detent force is different. However, the changing trends of cogging torque and detent force are the same.

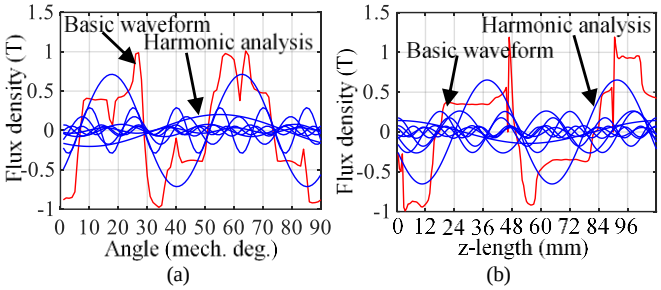

Fig. 10. Air-gap magnetic flux densities, (a) in the circumferential direction, and (b) in the axial direction.

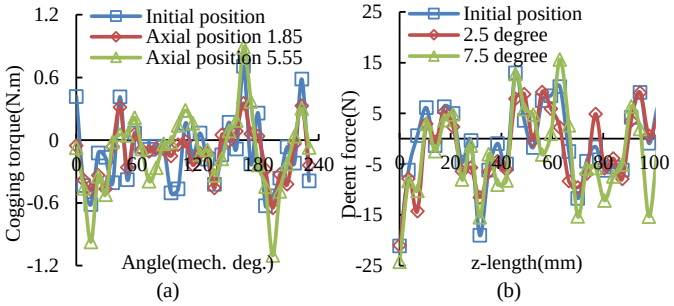

Fig. 11. Cogging torque and detent force of ES-LRMPMG, (a) rotary motion, and (b) linear motion when the mover is at different positions.

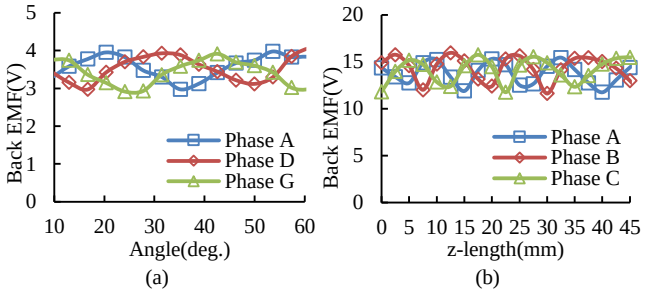

Fig. 12. Amplitude of back EMF waveforms when the mover is in different positions, (a) linear motion, and (b) rotary motion.

Fig. 12 shows the changing discipline of the amplitude value of back EMF waveforms when the mover is at different positions. The changing range of back EMF is from 2.8 V to 4 V when the motor works in linear motion under different mover positions in circumferential direction. The changing range of back EMF is from 11 V to 16.5 V when the motor works in rotary motion under different mover positions in axial direction. Therefore, the variation of back EMF is narrowed, and the voltage is easier to be stored. Fig. 13 shows back EMF waveforms of phase A when the motor works in rotary or linear motion and the mover is at different axial and circumferential positions. It can be seen that the amplitudes of nine phase back EMFs and the initial phase of phase A are the same, when the mover is at the same position whether it is in rotary or linear motion. According to the amplitude and initial phase of phase A, the amplitudes and initial phases of the other eight phases can be derived.

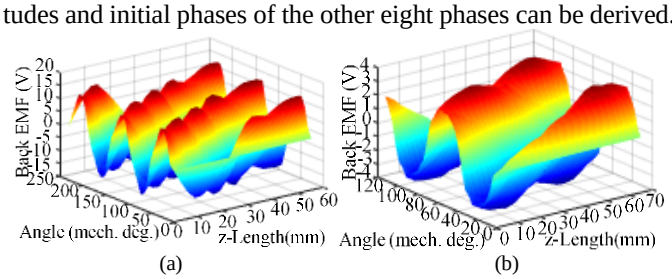

Fig. 13. Back EMF waveforms of phase A, (a) rotary motion when the mover is at different axial positions, and (b) linear motion when the mover is at different circumferential positions.

V. Conclusion

An ES-LRMPMG is proposed with single magnetic circuit structure, and the linear and rotary 2-DOF motions are achieved based on electromagnetic induction principle and transverse flux principle, respectively. The optimization design and electromagnetic characteristics are analyzed in the paper. Compared with the results of the initial topology, the harmonics of back EMF, the amplitudes of cogging torque and detent force are reduced after the optimization. Since the interlaced PM poles are staggered by half pole pitch in the axial direction, the initial phases of the windings (A, E, I), (B, F, G), and (C, D, H) are the same, and the variation range of back EMF amplitude value is narrowed when the mover is at different positions whether it works in rotary or linear motion, which is conducive to energy storage and improve the generation effectively.

References

[1] L. Xie, J. Si, Y. Hu, H. Feng, and K. Ni, "Characteristics analysis of the motions of the two-degree-of-freedom direct drive induction motor," *IEEE Trans. Ind. Electron.*, vol. 67, no. 2, pp. 931-941, Feb. 2020.

[2] O. Safdarzadeh, A. Mahmoudi, E. Afjei, and H. Torkaman, "Rotary-linear switched reluctance motor: analytical and finite-element modeling," *IEEE Trans. Magn.*, vol. 55, no. 5, May 2019, Art. no. 8200710.

[3] K. Guo, and Y. Guo, "Key parameter design and analysis of flux reversal linear rotary permanent magnet actuator," *IEEE Trans. Appl. Supercond.*, vol. 29, no. 2, Mar. 2019, Art. no. 0600405.

[4] K. Guo, Y. Guo, and J. Li, "Decoupling control analysis of a flux reversal linear rotary permanent magnet actuator," *Journ. Electron. Eng. Tech.*, vol. 15, no. 4, pp. 1693-1704, Jul. 2020.

[5] K. Guo, S. Fang, Y. Zhang, H. Yang, H. Lin, S. L. Ho, and N. Feng, "Irreversible demagnetization analysis of permanent magnet materials in a novel flux reversal linear-rotary permanent magnet actuator," *IEEE Trans. Magn.*, vol. 52, no. 7, pp. 1-4, Jul. 2016, Art. no. 8202904.

[6] S. Li, K. W. E. Cheng, N. Cheung, and Y. Zou, "Design and control of a decoupled rotary-linear switched reluctance motor," *IEEE Trans. Energy Convers.*, vol. 33, no. 3, pp. 1363-1371, Sep. 2018.

[7] Z. Zhang, H. Zhou, and J. Duan, "Design and analysis of a high acceleration rotary-linear voice coil motor," *IEEE Trans. Magn.*, vol. 53, no. 7, Jul. 2017, Art. no. 8203509.

[8] S. Miri´c, R. Giuffrida, D. Bortis, and J. W. Kolar, "Enhanced complex space vector modeling and control system design of multiphase magnetically levitated rotary-linear machines," *IEEE J. Emerg. Sel. Top. Power Electron.*, vol. 8, no. 2, pp. 1833-1849, Jun. 2020.

[9] T. J. Teo, H. Zhu, S. Chen, G. Yang, and C. K. Pang, "Principle and modeling of a novel moving coil linear-rotary electromagnetic actuator," *IEEE Trans. Ind. Electron.*, vol. 63, no. 11, pp. 6930-6940, Nov. 2016.